Spatial Propagation of Protein Polymerization

S. I. A. Cohen,[1,2] L. Rajah,[1] C. H. Yoon,[1] A. K. Buell,[1] D. A. White,[1] R. A. Sperling,[2] M. Vendruscolo,[1] E. M. Terentjev,[3] C. M. Dobson,[1,*] D. A. Weitz,[2,4,†] and T. P. J. Knowles[1,‡]

[1]*Department of Chemistry, University of Cambridge, Lensfield Road, Cambridge CB2 1EW, United Kingdom*
[2]*School of Engineering and Applied Sciences, Harvard University, Cambridge, Massachusetts 02138, USA*
[3]*Cavendish Laboratory, University of Cambridge, JJ Thomson Avenue, Cambridge CB3 0HE, United Kingdom*
[4]*Department of Physics, Harvard University, Cambridge, Massachusetts 02138, USA*

(Received 15 February 2013; published 4 March 2014)

We consider the spatial dependence of filamentous protein self-assembly. Through studying the cases where the spreading of aggregated material is dominated either by diffusion or by growth, we derive analytical results for the spatial evolution of filamentous protein aggregation, which we validate against Monte Carlo simulations. Moreover, we compare the predictions of our theory with experimental measurements of two systems for which we identify the propagation as either growth or diffusion controlled. Our results connect the macroscopic observables that characterize the spatial propagation of protein self-assembly with the underlying microscopic processes and provide physical limits on spatial propagation and prionlike behavior associated with protein aggregation.

DOI: 10.1103/PhysRevLett.112.098101 PACS numbers: 87.14.em, 87.15.nr, 87.15.rp, 87.15.Vv

Spatial patterns in soft matter systems are commonly generated through the growth of an aggregated phase within a soluble phase [1–4], for instance, as diffusion limited aggregation, or instead through the reaction and diffusion of components that remain in solution [5–8]. While the spatial distributions in many systems are characterized entirely by one of these two phenomena, the formation of filamentous aggregates from normally homogeneous protein solutions is made complex by the fact that it involves the growth within a soluble phase of structures that can diffuse and multiply in number.

The self-assembly of protein molecules into fibrillar structures is crucial for the generation of functional materials in nature, including the cytoskeleton [9], but it is also associated with the aberrant aggregation of normally soluble proteins into filamentous structures in the context of many pathologies, including sickle cell anemia [10] and amyloid disorders [11]. While phenomena involving reaction, diffusion, and growth have been of broad interest over the past several decades [1–8,12–14], biophysical studies of protein aggregation have focused primarily on the temporal evolution of the system concerned [9,15–17], rather than the spatial dependence that is associated with this phenomenon [18,19] and which is increasingly recognized as playing a key role in the ''prionlike'' pathology of various protein misfolding disorders [20–22].

The conversion of soluble proteins into linear polymers involves the homogeneous (primary) nucleation of nascent aggregates, which are able to grow by incorporating further monomers at their ends [9]. Moreover, existing aggregates often accelerate the rate of generation of further aggregates through fragmentation [16] and heterogeneous nucleation [15], processes that are collectively known as secondary pathways [23]. Fragmentation refers to the breakage of a filament to give two daughter aggregates, whereas heterogeneous (secondary) nucleation occurs when the surfaces of filaments catalyze the nucleation of further aggregates from the soluble protein. In macroscopic volumes, the overall polymerization reaction is the result of many individual primary nucleation events and subsequent elongation and secondary processes that affect the resulting aggregates [23]. In this case, an approach that averages over the volume and neglects the spatial dependence can be appropriate for describing this phenomenon [17,23]. On a cellular scale, however, the aggregation reaction can correspond to propagation from a single, or a small number of, primary nucleation event(s) [19], which are then amplified by elongation and secondary pathways. In this context, therefore, it is vital to characterize the spatial propagation from discrete homogeneous nucleation events.

As a protein polymerization reaction progresses from a single nucleation event, the resulting aggregates propagate through space both due to the diffusion of aggregates [Fig. 1(a)] and through the growth of aggregates at their ends to occupy additional space [Fig. 1(c)]. Here, we probe the spatial propagation of the protein self-assembly reaction in the limits where each of these two mechanisms is dominant, in order to reveal the link between the microscopic processes underlying protein aggregation and the macroscopic observables that characterize the spreading of the aggregated material.

Propagation through diffusion.—When spatial propagation is controlled primarily by the diffusion of aggregates, rather than by their growth, the master equation [24] for the field $f(t, \mathbf{r}, j)$, which describes the population length distribution of aggregates consisting of j monomers, is given as

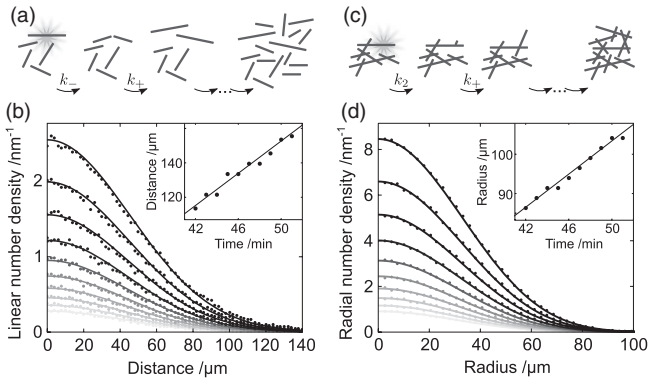

FIG. 1. (a),(c) Schemas of the two modes of spatial propagation considered here. In (a), aggregates spread primarily through diffusion while they grow through elongation and multiply through a secondary pathway (illustrated as filament fragmentation). In (c), the aggregates instead spread primarily through their growth, as they multiply through a secondary pathway (illustrated as secondary nucleation). The fragmentation and secondary nucleation events are highlighted with stars. (b), (d) Comparison of the corresponding analytical results (solid lines) and the results of Monte Carlo simulations [28] (data points) for the concentration profiles at increasing times. Panel (b) shows the linear number density $\int dy \int dz P$ from (3) for diffusion, and panel (d) shows the radial density $4\pi r^2 P$ from (7) for radial spreading through growth. The insets show the farthest position where a threshold density, $\theta = 5\ \mu\mathrm{m}^{-1}$, is reached in the numerical concentration profiles (data points); the front velocity is given by the slope and compared to the analytical results (solid lines) derived in the text. The parameters are $k_+ = 9 \times 10^4\ \mathrm{M}^{-1}\,\mathrm{s}^{-1}$, $m = 5$ mM, $k_- = k_2 m^{n_2} = 2 \times 10^{-8}\ \mathrm{s}^{-1}$ in (b) and (d) respectively, giving a ratio $S = 2.2$ of the diffusion to growth controlled propagation velocities. The prefactors were $\delta = 1$ Å, $\eta = 0.5$ mPa s, $d = 8$ nm, $T = 330$ K.

$$\frac{\partial f(t,\mathbf{r},j)}{\partial t} = 2mk_+ f(t,\mathbf{r},j-1) - 2mk_+ f(t,\mathbf{r},j) - k_-(j-1)f(t,\mathbf{r},j) + 2k_- \sum_{i=j+1}^{\infty} f(t,\mathbf{r},i) + k_2 m^{n_2}\delta_{j,n_2} \sum_{i=n_2}^{\infty} i f(t,\mathbf{r},i) + D(j)\nabla^2 f(t,\mathbf{r},j), \tag{1}$$

where m is the concentration of monomeric protein, $D(j)$ is the orientationally averaged diffusion coefficient of an aggregate of j monomers, and k_+, k_-, and k_2 are the rate constants for elongation, fragmentation, and secondary nucleation, respectively. The first term in (1) accounts for the formation of aggregates of size j through the elongation of aggregates of size $j-1$, while the second term describes the loss of aggregates of size j through their elongation [9]. The third and fourth terms relate to the loss or generation of an aggregate of size j through fragmentation [16], and the fifth term accounts for the secondary nucleation of an aggregate of size n_2 at a rate proportional to the surface area of the aggregates [15]. The final term describes the spatial diffusion of aggregates. Primary nucleation is not included in (1) since we consider here the propagation of aggregates following a single primary nucleation event at the coordinate origin. We consider the case where the monomer is not significantly depleted such that m is constant in space and time [23].

The size-dependent orientationally averaged translational diffusion coefficient of a filamentous protein aggregate is required in (1); for a high-aspect ratio rigid rod of length L and diameter d, this is given by $D = k_B T/(6\pi\eta R_h)$, where the effective hydrodynamic radius $R_h \approx \gamma L$ for $\gamma^{-1} = 2\log(2L/d)$ [25]. Since γ depends only logarithmically on the length L, the hydrodynamic radius R_h varies approximately linearly, and the diffusion coefficient D varies approximately inversely, with the filament length over a wide range of lengths.

The evolution of the lower moments of the length distribution of filaments, the number concentration $P(t,\mathbf{r}) = \sum_{j=n_c}^{\infty} f(t,\mathbf{r},j)$, and the mass concentration $M(t,\mathbf{r}) = \sum_{j=n_c}^{\infty} j f(t,\mathbf{r},j)$, which are the principal experimental observables, are determined from the master equation (1) through summation [16]. For the mass concentration, this yields [26–28]

$$\frac{\partial M(t,\mathbf{r})}{\partial t} = \kappa\mu P(t,\mathbf{r}) + \bar{D}\mu\nabla^2 P(t,\mathbf{r}), \tag{2}$$

where the parameter $\kappa = \sqrt{2mk_+(k_- + k_2 m^{n_2})}$ is the proliferation rate that emerges in the spatially homogeneous case [16,24]. Similarly, the unitless parameter $\mu = 2k_+ m/\kappa$ has the physical interpretation as the average polymerization number of filaments that emerges from (1) after times $t \gg \kappa^{-1}$ when the spatial dependence is neglected [29]. Indeed, even when diffusion is active, the local length distribution at each point will approach that given in the spatially homogeneous case [29], under the condition that the length distribution reaches equilibrium over a time scale much shorter than that in which aggregates diffuse a distance comparable with their size, i.e., $\kappa^{-1} \ll \bar{D}^{-1}(\mu\delta)^2$. This condition results in the approximation $P(t,\mathbf{r}) \approx M(t,\mathbf{r})/\mu$, under which (2) then describes reaction-diffusion growth [30]. The effective diffusion coefficient in (2) is $\bar{D} = [kT/(6\pi\eta\bar{\gamma}\delta)]\sqrt{(k_- + k_2 m^{n_2})/(2k_+ m)}$, where γ is approximated using the mean length $L = \delta\mu$ to yield $\bar{\gamma}^{-1} = 2\log(2\delta\mu/d)$, and the length of an aggregate of size j is given as $L = \delta j$ for an extension δ corresponding to each monomer. Since the rate constants for fragmentation and secondary nucleation enter into the analysis additively in (2), from here on we replace $(k_- + k_2 m^{n_2})$ with $k_2 m^{n_2}$ and note that the case of fragmenting filaments is accounted for when $k_2 = k_-$ and $n_2 = 0$ [24].

In the present case of propagation from a single nucleus at the coordinate origin, the resulting aggregation process cannot be detected until the initial nucleus has grown and multiplied to reach an experimental detection threshold. The spatial distribution of aggregates when detection is possible will then be centered on a location $\mathbf{r_0}$ that

corresponds to a stochastic spatial offset resulting from the diffusion of the initial aggregate(s) for times $t < t_0 \sim \kappa^{-1}$ before significant multiplication. The solution for the reaction-diffusion dynamics described by (2) is then given by

$$P(t + t_0, \mathbf{r} + \mathbf{r_0}) = \frac{\exp(\kappa t - \frac{r^2}{4\bar{D}t})}{\sqrt{4\pi\bar{D}t}}. \quad (3)$$

The resulting behavior is dominated by the exponential factor; the spatial position at which an arbitrary detection threshold level, $P = \theta$, is reached is given as $r_\theta = ut[1 - 4\bar{D}\log(\theta\sqrt{4\bar{D}t})/(u^2 t)]^{1/2} \overset{t\gg 1}{\rightarrow} ut$ for the velocity of the reaction front $u = 2\sqrt{\bar{D}\kappa}$, i.e., a Fisher wave [30]. Combining this result with the identification of $\bar{D}$ and κ as functions of the microscopic rate constants reveals that in this case the reaction front propagates outwards from the origin with a velocity $u = \sqrt{2k_2 m^{n_2} k_B T/(3\pi\eta\tilde{\gamma}\delta)}$, which is dependent only on the rate of the secondary process and not on the elongation rate of the filaments. Furthermore, for the breakage dominated case ($k_2 = k_-$, $n_2 = 0$), the wave velocity is concentration independent. The analytical forms for the concentration profiles (3) are compared with numerical data from Monte Carlo simulations of this process in Fig. 1(b), demonstrating the accuracy of the analytical approximation.

Propagation through growth.—Since the self-assembly reaction also involves mass transport, it is crucial to consider the converse limit where spreading is dominated by the movement of filament ends upon aggregate growth. Specifically, we consider the radial growth of a spherical filament network wherein individual aggregates are unable to diffuse. This situation is analogous to the growth of domains of aggregated hemoglobin *S* in sickle cell disease, which has been studied by Ferrone and co-workers [18]. Following this approach, we describe the state of the system with three variables: the local polymer mass concentration $M(t, r)$ and the local concentrations of filament ends $E^{\pm}(t, r)$ pointing towards $\pm r$ (radial outward or inward). The time evolution of the number of ends in each direction due to growth can be obtained by noting that, within a spherical shell of thickness dr,

$$4\pi r^2 dr\delta E^{\pm}_{\text{elongation}}(t, r) = \mp 4\pi r^2 E^{\pm}(t, r)\upsilon dt \pm 4\pi(r - dr)^2 \times E^{\pm}(t, r - dr)\upsilon dt, \quad (4)$$

where $\upsilon = 2mk_+\delta/\pi$ is the average projected elongation velocity of the filament assuming random directionality of growth [18]; the factor of $2/\pi$ originates from the average projection $\langle\cos(\theta)\rangle = 2/\pi$. Taking the limit $dr \rightarrow 0$, $dt \rightarrow 0$ of (4), and adding to this case the effect of secondary pathways $\delta E^{\pm}_{\text{nucleation}}(r) = k_2 m^{n_2} M$, yields the partial differential equation for the evolution of the number of filament ends pointing in each direction:

$$\frac{\partial E^{\pm}(t, r)}{\partial t} = \mp\frac{2mk_+\delta}{\pi r^2}\frac{\partial}{\partial r}(r^2 E^{\pm}(t, r)) + k_2 m^{n_2} M(t, r). \quad (5)$$

Since there is no significant diffusion of aggregates, the mass concentration evolves as $\partial_t M = mk_+(E^+ + E^-) = 2Pmk_+$ [(2) with $\bar{D} = 0$], where we have identified the aggregate number concentration with half the number of filament ends, $P = (E^+ + E^-)/2$. Taking the sum and the difference of the two expressions in (5) for $E^{\pm}$ gives coupled equations for $(E^+ + E^-)$ and $(E^+ - E^-)$; eliminating the latter term through differentiation [31], and substituting for the time evolution of the mass concentration on the right-hand side, gives a decoupled equation for the number concentration P:

$$\frac{\partial^2}{\partial t^2}P(t, r) = \frac{\upsilon^2}{r^2}\frac{\partial^2}{\partial r^2}(r^2 P(t, r)) + \kappa^2 P(t, r), \quad (6)$$

with the effective multiplicative rate $\kappa = \sqrt{2k_+ k_2 m^{n_2+1}}$, as in (2). Equation (6) is a Klein-Gordon equation in $r^2 P$ with an imaginary mass term, also known as the modified telegrapher's equation. The solution corresponding to a single aggregate initially at the origin is

$$P(t + t_0, \mathbf{r} + \mathbf{r_0}) = \frac{1}{2\pi\delta\mu}\frac{\upsilon t}{r^2\sqrt{t^2\upsilon^2 - r^2}} I_1\left(\frac{\kappa}{\upsilon}\sqrt{t^2\upsilon^2 - r^2}\right), \quad (7)$$

for $r < \upsilon t$ and $P = 0$ for $r > \upsilon t$; the nth modified Bessel function of the first kind is denoted I_n. Offsets in space and time are added as for (3). Equation (7) may then be integrated to yield the mass concentration:

$$M(t + t_0, \mathbf{r} + \mathbf{r_0}) = \frac{1}{4\pi\delta r^2} I_0\left(\frac{\kappa}{\upsilon}\sqrt{t^2\upsilon^2 - r^2}\right). \quad (8)$$

The velocity associated with the reaction front, $\upsilon = 2mk_+\delta/\pi$, depends in this case only on the rate of elongation, and not on the rate of secondary nucleation. The accuracy of the analytical results is verified by means of numerical simulations, shown in Fig. 1(d).

Experimental realizations of propagation through diffusion and growth.—We apply the results derived in this Letter to two experimental situations, both involving the aggregation of a representative amyloid forming protein, insulin, which has been found to involve homogeneous nucleation, elongation, and filament fragmentation under defined conditions [16,28]. We utilize microfluidic techniques which allow us to directly observe the spatial propagation of aggregates resulting from discrete homogeneous nucleation events [28]. We focus first on conditions where both of the propagation modes derived in this Letter are accessible, by considering the propagation of insulin aggregates growing from single nuclei confined in high-aspect ratio microdroplets [19], Figs. 2(a) and 2(b). We then study aggregation under conditions where diffusion is severely disfavored, by investigating the growth of spherulites [32]; in these higher-order spherical structures, which nucleate preferentially in contact with the microchannel walls, the diffusion of insulin filaments is significantly hindered, Figs. 2(c) and 2(d).

The progression of representative experiments of each type is shown in Figs. 2(a) and 2(c). The rate of spreading between consecutive images in both cases is approximately constant, implying constant propagation velocities. Quantitative analyses of the propagation velocities from several series of experimental images are shown in Figs. 2(b) and 2(d), verifying in all cases that the propagation velocities are constant in time, as predicted by (3) and (7). It is interesting to note that the measured propagation velocities shown in Fig. 2(b), where both diffusion and growth occur, are 2 orders of magnitude greater than in Fig. 2(d), where propagation is through growth and there is minimal diffusion; this observation confirms that diffusion, rather than growth, is primarily responsible for the propagation of insulin polymerization shown in Figs. 2(a) and 2(b).

The analytical results for the velocity of the reaction front in the two cases discussed in this Letter have strikingly different dependencies on the microscopic rate constants of aggregation. For spreading through diffusion, the velocity depends only on the rate constant of the secondary pathway and not on the elongation rate constant; a precisely converse dependency emerges for propagation through growth. An intriguing prediction of these results, therefore, is that if one of these two rate constants is altered, the front velocity will only be affected either in a system with a dominant diffusive mode of propagation or in a system with growth controlled propagation.

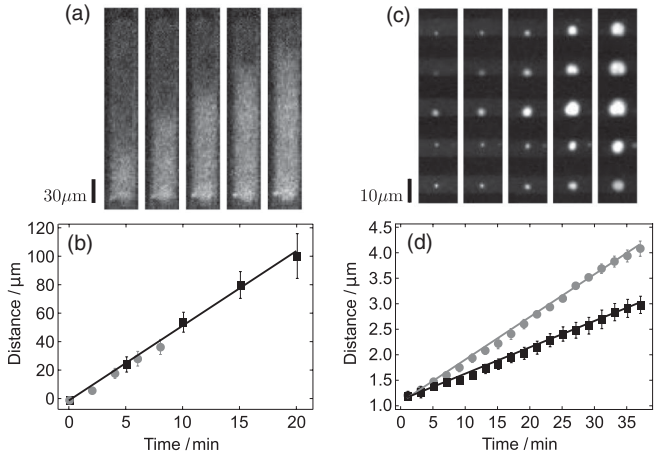

FIG. 2. Representative images of the progression over time of experiments [28] involving diffusion (a) and growth (c) dominated propagation of insulin aggregation, as described in the text. In both cases, aggregation was monitored by means of the fluorescent probe thioflavin T, which has a high affinity for the amyloid scaffold [16]. (a) Single microdroplet and (c) five spherulites. (b),(d) Corresponding measurements of the velocity of the reaction fronts for these systems at two different concentrations of NaCl (black, 0 mM; gray, 10 mM; both in the presence of 50 mM HCl). Note that the velocity in (a) and (b) is much greater than in (c) and (d), consistent with the fact that the propagation in (a) and (b) is controlled by diffusion and not growth. In addition, note that the growth of a dense crystal phase would not result in a volume filling process as observed in (a), since only a small volume fraction, ~3% in our experiments, is protein.

In order to test this prediction, experiments under both conditions in Fig. 2 were carried out at two different concentrations of sodium chloride (0 mM, 10 mM). This difference in salt concentrations is known to affect the elongation rate [33] but is not expected to affect the rate of fragmentation, implying that only the propagation velocity for spreading dominated by growth should be affected. The data for the front velocities in Fig. 2 show clearly that under conditions where propagation is primarily through diffusion, Fig. 2(b), a change in salt concentration has no detectable effect on the velocity, whereas under the conditions where propagation occurs through growth, Fig. 2(d), an increase in salt concentration results in a very significant change in the velocity. Moreover, the analytical result for the conditions where the velocity is limited by growth indicates that the ratio of the velocities measured in Fig. 2(d) should be equal to the ratio of the elongation rate constants; the ratio of the slopes in Fig. 2(d) is approximately 1.7, which is consistent with previous values of the change in the elongation rate for insulin due to a 10 mM increase in ionic strength on a background ionic strength of 50 mM [33].

A dimensionless parameter, S, that quantifies whether propagation is driven by diffusion ($S > 1$) or growth ($S < 1$) can be constructed as the ratio of the respective velocities:

$$S = \sqrt{\frac{k_2 m^{n_2-2} k_B T \pi}{6 k_+^2 \eta \tilde{\gamma} \delta^3}}, \tag{9}$$

where values of the prefactors δ, η, $\bar{\gamma}$, T for the growth of amyloid fibrils [34] result in $S \approx (10^7 s^{-1/2}) k_2^{1/2} \times m^{n_2/2-1}/k_+$. In the case of insulin, we have previously determined the rate constants [16,34,35] ($n_2 = 0$, $k_2 = k_- \approx 10^{-8}$ s^{-1}, $k_+ m \approx 10$ s^{-1} [36]), resulting in $S \approx (10^7 s^{-1/2}) k_-^{1/2}/(k_+ m) \approx 100$, in excellent agreement with the ratio of the diffusion (~ 5 μm min^{-1}) to the growth (~ 0.05 μm min^{-1}) controlled velocities measured in Fig. 2.

It is interesting to speculate, therefore, that diffusive propagation may be a key mode of spreading for a range of situations involving the formation and proliferation of amyloid fibrils, including those related to disease. In agreement with this idea, it is increasingly apparent that the spatial spreading of protein aggregation processes from cell to cell in the central nervous system, initially established only for prion conditions, is more generally associated with the onset and progression of a wide class of neurodegenerative disorders, including Alzheimer's and Parkinson's diseases [20,37–40]. In particular, low molecular weight aggregates of the amyloid-β (Aβ) peptide, sometimes called Aβ-related diffusible ligands, are implicated in the pathogenesis of Alzheimer's disease [41]. The ability to sustain spatial propagation through diffusion may be enhanced for these low molecular weight species since they are commonly observed to have low growth rates relative to elongated fibrils [42–44]. Interestingly, since our data show that secondary pathways control the velocity of diffusive propagation, these findings suggest that such

processes, which are already thought to be important in many cases for generating low molecular weight species [16,45], may also be crucially important for controlling their spatial spreading and associated prionlike behavior [20–22].

We thank D. R. Nelson and M. P. Brenner for helpful discussions. This work was supported by the Schiff Foundation (S. I. A. C.), the Kennedy Memorial Trust (S. I. A. C.), the Wellcome Trust (M. V., C. M. D., T. P. J. K.), the Newman Foundation (T. P. J. K.), and the BBSRC (T. P. J. K.).

*cmd44@cam.ac.uk
†weitz@seas.harvard.edu
‡tpjk2@cam.ac.uk

[1] A. J. Hurd and D. W. Schaefer, Phys. Rev. Lett. **54**, 1043 (1985).
[2] E. Brener, H. Levine, and Y. Tu, Phys. Rev. Lett. **66**, 1978 (1991).
[3] K. V. Klenin, H. Merlitz, J. Langowski, and C.-X. Wu, Phys. Rev. Lett. **96**, 018104 (2006).
[4] N. Dorsaz, C. De Michele, F. Piazza, P. De Los Rios, and G. Foffi, Phys. Rev. Lett. **105**, 120601 (2010).
[5] J. L. Spouge, Phys. Rev. Lett. **60**, 871 (1988).
[6] E. Khain and L. M. Sander, Phys. Rev. Lett. **96**, 188103 (2006).
[7] X. Yuan, H. Wang, and Q. Ouyang, Phys. Rev. Lett. **106**, 188303 (2011).
[8] J. S. Bois, F. Jülicher, and S. W. Grill, Phys. Rev. Lett. **106**, 028103 (2011).
[9] F. Oosawa and S. Asakura, *Thermodynamics of the Polymerization of Protein* (Academic Press, New York, 1975).
[10] F. A. Ferrone, Microcirculation **11**, 115 (2004).
[11] F. Chiti and C. M. Dobson, Annu. Rev. Biochem. **75**, 333 (2006).
[12] A. J. C. Ladd, H. Gang, J. X. Zhu, and D. A. Weitz, Phys. Rev. Lett. **74**, 318 (1995).
[13] R. C. Ball and E. Somfai, Phys. Rev. Lett. **89**, 135503 (2002).
[14] A. Menshutin, Phys. Rev. Lett. **108**, 015501 (2012).
[15] F. A. Ferrone, J. Hofrichter, and W. A. Eaton, J. Mol. Biol. **183**, 611 (1985).
[16] T. P. J. Knowles, C. A. Waudby, G. L. Devlin, S. I. A. Cohen, A. Aguzzi, M. Vendruscolo, E. M. Terentjev, M. E. Welland, and C. M. Dobson, Science **326**, 1533 (2009).
[17] S. I. A. Cohen, M. Vendruscolo, C. M. Dobson, and T. P. J. Knowles, J. Mol. Biol. **421**, 160 (2012).
[18] H. X. Zhou and F. A. Ferrone, Biophys. J. **58**, 695 (1990).
[19] T. P. J. Knowles, D. A. White, A. R. Abate, J. J. Agresti, S. I. A. Cohen, R. A. Sperling, E. J. D. Genst, C. M. Dobson, and D. A. Weitz, Proc. Natl. Acad. Sci. U.S.A. **108**, 14 746 (2011).
[20] A. Aguzzi and J. Falsig, Nat. Neurosci. **15**, 936 (2012).
[21] M. Jucker and L. C. Walker, Ann. Neurol. **70**, 532 (2011).
[22] M. Jucker and L. C. Walker, Nature (London) **501**, 45 (2013).
[23] F. Ferrone, Methods Enzymol. **309**, 256 (1999).
[24] S. I. A. Cohen, M. Vendruscolo, M. E. Welland, C. M. Dobson, E. M. Terentjev, and T. P. J. Knowles, J. Chem. Phys. **135**, 065105 (2011).
[25] M. Doi and S. F. Edwards, *The Theory of Polymer Dynamics* (Oxford University Press, Oxford, England, 1986).
[26] The diffusion coefficient is of the form $D \sim j^{-1} \log j$; in the moment equation for $M = \sum j f(t, \mathbf{r}, j)$ only the weak $\log j$ dependency remains and hence approximating $\log j \approx \log \mu$ leads to a good approximation.
[27] Terms describing the direct effect of nucleation on the aggregate mass are neglected in Eq. (2) since the major role of nucleation is to generate additional sites for elongation [23,24]. Were the opposite true, large aggregates would not form.
[28] See Supplemental Material at http://link.aps.org/supplemental/10.1103/PhysRevLett.112.098101 for a detailed derivation of Eq. (2) and additional experimental and simulation details.
[29] S. I. A. Cohen, M. Vendruscolo, C. M. Dobson, and T. P. J. Knowles, J. Chem. Phys. **135**, 065107 (2011).
[30] P. Grindrod, *The Theory and Applications of Reaction-Diffusion Equations* (Oxford University Press, Oxford, England, 1996).
[31] Taking the difference between the expressions for $E^{\pm}$ in Eq. (5) yields $\partial_t(E^+ - E^-) = -2mk_+\delta\partial_r(r^2[E^+ + E^-])/(\pi r^2)$, whereas adding the expressions for $E^{\pm}$ then differentiating with respect to time yields $\partial_{tt}(E^+ + E^-) = -2mk_+\delta\partial_r\{r^2\partial_t([E^+ - E^-])\}/(\pi r^2) + 2k_2m^{n_2}\partial_t M$. Eliminating $\partial_t(E^+ - E^-)$, and substituting $\partial_t M = 2mk_+P$, results in Eq. (5).
[32] M. R. H. Krebs, C. E. Macphee, A. F. Miller, I. E. Dunlop, C. M. Dobson, and A. M. Donald, Proc. Natl. Acad. Sci. U.S.A. **101**, 14 420 (2004).
[33] A. K. Buell, P. Hung, X. Salvatella, M. E. Welland, C. M. Dobson, and T. P. J. Knowles, Biophys. J. **104**, 1116 (2013).
[34] J. F. Smith, T. P. J. Knowles, C. M. Dobson, C. E. Macphee, and M. E. Welland, Proc. Natl. Acad. Sci. U.S.A. **103**, 15 806 (2006).
[35] A. K. Buell, J. R. Blundell, C. M. Dobson, M. E. Welland, E. M. Terentjev, and T. P. J. Knowles, Phys. Rev. Lett. **104**, 228101 (2010).
[36] At the high concentration, 5 mM, of insulin used in our experiments, the elongation rate no longer varies linearly with the monomer concentration as k_+m but rather approaches a saturated rate, which is independent of the monomer concentration, corresponding to the time scale for rearrangement when a monomer attaches to a fibril end [35]. The limiting rate is used in this calculation.
[37] J.-Y. Li *et al.*, Nat. Med. **14**, 501 (2008).
[38] K. C. Luk, V. Kehm, J. Carroll, B. Zhang, P. O'Brien, J. Q. Trojanowski, and V. M.-Y. Lee, Science **338**, 949 (2012).
[39] P. Brundin, R. Melki, and R. Kopito, Nat. Rev. Mol. Cell Biol. **11**, 301 (2010).
[40] S.-J. Lee, P. Desplats, C. Sigurdson, I. Tsigelny, and E. Masliah, Nat. Rev. Neurol. **6**, 702 (2010).
[41] C. Haass and D. J. Selkoe, Nat. Rev. Mol. Cell Biol. **8**, 101 (2007).
[42] N. Cremades *et al.*, Cell **149**, 1048 (2012).
[43] T. R. Serio, A. G. Cashikar, A. S. Kowal, G. J. Sawicki, J. J. Moslehi, L. Serpell, M. F. Arnsdorf, and S. L. Lindquist, Science **289**, 1317 (2000).
[44] J. Lee, E. K. Culyba, E. T. Powers, and J. W. Kelly, Nat. Chem. Biol. **7**, 602 (2011).
[45] S. I. A. Cohen, S. Linse, L. M. Luheshi, E. Hellstrand, D. A. White, L. Rajah, D. E. Otzen, M. Vendruscolo, C. M. Dobson, and T. P. J. Knowles, Proc. Natl. Acad. Sci. U.S.A. **110**, 9758 (2013).